Lubrication Science

Studies of Inherent Lubricity Coatings for Low Surface Roughness Galvanized Steel for Automotive Applications

Journal:	*Lubrication Science*
Manuscript ID	LS-16-0083-RA-LS.R1
Wiley - Manuscript type:	Research Article - LS
Date Submitted by the Author:	n/a
Complete List of Authors:	Hill, Donald; Swansea University, Engineering Holliman, Peter; Bangor University, School of Chemistry McGettrick, James; Swansea University, Engineering Searle, Justin; Swansea University, Engineering Appleman, Marco; Tata Steel Research Development and Technology Chatterjee, Pranesh; Tata Steel Research Development and Technology Watson, Trystan; Swansea University, Engineering Wprsley, David; Swansea University, Engineering
Keywords:	
New Keyword Selection:	Coatings < Self-lubricating Materials < Lubricant Synthesis (Focus on Material), Solid Lubricants < Self-lubricating Materials < Lubricant Synthesis (Focus on Material), Chemical Analysis < Analysis < Lubricant Analysis and Diagnostics (Focus on Methods), Physical Analysis < Analysis < Lubricant Analysis and Diagnostics (Focus on Methods), Surface-sensitive Techniques < Tribo-chemistry < Lubrication Performance and Tribo-chemistry

Studies of Inherent Lubricity Coatings for Low Surface Roughness Galvanized Steel for Automotive Applications

Donald Hill[a], Peter J. Holliman[b,*], James McGettrick[a], Justin Searle[a], Marco Appelman[c], Pranesh Chatterjee[c], Trystan M. Watson[a] and David Worsley[a].

[a] SPECIFC, College of Engineering, Swansea University, Baglan, Port Talbot, SA12 7AX, UK
[b] School of Chemistry, Bangor University, Bangor, Gwynedd LL57 2UW, UK
[c] TATA Research & Development 1970 CA IJmuiden
p.j.holliman@bangor.ac.uk

Sponsors
We gratefully acknowledge funding from EPSRC EngD and Tata Steel (DH), the Welsh Government for Sêr Cymru (PJH) and EPSRC/InnovateUK EP/I019278/1 (JMc, JS).

Abstract
Surface lubricity on TiO_2-coated galvanized steels can be controlled by solution depositing perfluorooctanoic (**C8**), lauric (**C12**) or stearic (**C18**) acids to avoid lubricating oils/emulsions or substrate pre-etching to remove surface oxide which add cost and waste. Water contact angles (WCA) reveal increased surface hydrophobicity on coated samples which correlate with linear friction testing (LFT) suggesting WCA can be used to screen lubricity compounds. LFT shows that **C12** and **C18** lower the coefficient of friction (μ) by 50-60% compared to uncoated substrates whilst **C8** drops μ from 0.31 to 0.22. Surfaces have been characterized by XPS, SEM and AFM whilst IR confirms that as-deposited coatings contain physisorbed and deprotonated acids chemisorbed through esters and TGA confirms increasing loadings from **C8** to **C12** to **C18**. Surface washing removes physisorbed material and lowers μ by increasing surface organization and alkyl chain packing which enhances frictional energy dissipation through steric quenching.

Keywords: Lubricity; Friction; Sorption; Automotive steel; Sheet metal forming

1. Introduction

Galvanized steel is formed into complex shapes for vehicle bodies through techniques such as deep drawing which relies on material ductility to create new shapes as the substrate is forced over tools by the mechanical action of a punch[1,2]. Adequate lubrication is essential to reduce friction to avoid wear on the substrate surface caused by frictional force at the interface between the substrate and the shaping tools[3]. Currently, drawing oils, emulsions or colloids are deposited onto automotive steels by spray, roll or drip coating to act as deep drawing lubricants[4]. Whilst these emulsions are non-toxic, they rely on the surface texture of the substrate to remain in place during

forming[5]. However, the poorer paint finish which can result from surface roughness[6] means the automotive sector is increasingly driving towards smoother substrates.

Consequently, there is a need to develop alternative lubricants which can operate at a wider range of surface texture specifications of automotive steels. Conformal deposition at a molecular level avoids macro-surface roughness issues because it operates at an entirely different length scale (pm compared to μm). Previously, low surface energy monolayers have been used to generate low friction surfaces on different materials; e.g. stearate on Al[7] or steel[8,9], silanes on Si[10] or phosphonates on Cu[11]. In general, the organic molecules that form such monolayers contain linker groups that bind to substrate surface atoms and alkyl chains that orient away from the surface to reduce interfacial shear forces[12]. However, prior reports for the surface functionalize metals or metal oxides have often used pre-treatments such as polishing[13] or plasma cleaning[8] to generate homogeneous, ultra-clean and/or oxide-free surfaces. In a laboratory, these approaches work well but, on a production line, these extra steps increase cost and waste. Thus, we have taken the opposite approach and, rather than remove surface oxide, we have studied the self-assembly of carboxylic acids either onto pre-cast TiO_2 films or, where there is incomplete TiO_2 surface coverage, directly onto the native ZnO surface layer of galvanized steel. We have chosen to use study the addition of a TiO_2 layer onto the galvanised substrate because carboxylic acids have been observed to chemisorb as monolayers onto metal oxide surfaces (e.g. TiO_2) through ester linkages[14-15] in a similar way to that used in dye-sensitized solar cells[16-17].

In this paper, we report studies of using stearic, lauric or perfluorooctanoic acid to generate cost effective, low toxicity, processable films with controlled surface lubricity on low surface roughness, galvanized automotive steel. Whilst low friction, stearate films have been reported on Al[7], steel[8,9,13], and mica[19], to our knowledge, lauric and perfluorooctanoic acid have not been studied in this context. We have linked detailed characterization of these surfaces with coefficient of friction (μ) and contact angle data. Whilst correlations between atomic force microscopy friction coefficients and contact angle data have been reported for glass substrates[18], we also report the first attempts to determine whether such a correlation exists for galvanized steel substrates as such correlation would enable contact angle measurements to be used as screening methods for compounds that could imbue surface lubricity.

2. Materials and Methods

2.1 Samples and chemicals

Galvanized steel (DX56, Tata Steel) was cut into 10×20 mm^2 coupons for characterization and 50×300 mm^2 strips for linear fiction testing. The steel composition (% wt) was Al 0.036, C 0.0022, Mo 0.001, Ni 0.001, N 0.0035, P 0.009, Si 0.003, S 0.010, Sn 0.004, Ti 0.050, V 0.002, Cr 0.012, Cu 0.026, Mn 0.088, B 0.002 and the balance was Fe. The surface roughness was 0.97 ± 0.05 μm; measured using a Marsurf profilometer. All other chemicals were sourced from Sigma Aldrich and used without further purification.

2.2 Surface functionalization

Samples were air dried after each of the following steps. Surface oil was removed from the steel by scrubbing with water and detergent and then ultra-sonicating in acetone for 5min. Selected substrates were immersed in an isopropanolic solution of $Ti(OPr)_4$ (10mM) for 30s. Substrates were then immersed in 100 mM isopropanolic solutions of the carboxylic acids for 30s before analysis. Selected samples were then either rinsed with acetone for 2 min or immersed in 100mM $NaOH_{(aq)}$ for 30s.

2.3 Characterization

Contact angle measurements (n = 5, 5µl D.I. water) were made using the sessile drop technique with a USB 2.0 camera and goniometer and the data were fitted using FTA 32 software (FTA 32 Europe). IR spectra (4 scans, $4cm^{-1}$ resolution) were recorded on a Perkin Elmer 100 Series ATR-FTIR spectrometer, between 650 and $4000cm^{-1}$. Field emission gun scanning electron microscopy (FEG-SEM) was carried out on a Hitachi S4800 at 1.0kV ($J_{emission}$ = 5µA, working distance = 11.5mm). Energy dispersive X-Ray (EDX) spectra were recorded using a Silicon Drift X-Max EDX detector and Inca EDX software (Oxford Instr.) at 15.0kV ($J_{emission}$ = 15µA, working distance = 17.0mm, acquisition = 100s). AFM data were measured over 10 x 10 µm scan areas on a JPK Nanowizard 3 AFM in contact mode using a Si tip (thickness 3 µm, length 225 µm) with a force constant of 2.8 N m^{-1}. The tip velocity was 20 µm s^{-1} with a line rate of 0.5 Hz. X-Ray photoelectron spectra (XPS) were recorded on an Axis Supra XPS (Kratos Analytical) using a monochromated Al K_α source and large area slot mode detector (300 x 800µm analysis area). Data were recorded using a charge neutralizer to limit differential charging and binding energies were calibrated to the main hydrocarbon peak (BE 284.8 eV). For each etch, a survey scan was recorded using a pass energy of 160eV. Data were fitted using CASA software with Shirley backgrounds. A 0.1 eV step size was used when recording the high resolution spectra and a pass energy of 20 eV. Thermal gravimetric analysis (TGA) data were recorded on a Pyris 1 TGA, heating from 25 ^oC to 550^oC at 25 $^oCmin^{-1}$ under N_2 (20 $mlmin^{-1}$). Coefficients of friction were measured using linear friction testing (LFT), a strip drawing test similar to that reported by Trzepiecinski *et al.*[20] at 22-24^oC and 30-45% RH (ESI Fig. 1). To do this, samples (50x300mm, n = 3) were pulled between round and cylindrical tools, clamped together with a force of 5kN, at 0.345mms^{-1} for a track length of 60mm. This sliding speed is slower than that typically used in deep drawing but was used to invoke very high friction to cause much faster removal of the zinc layer. Otherwise the tests would have required prohibitively very large amounts of material to study LFT. A new tool pair was used for each LFT test. The pulling force was measured and used to calculate the coefficient of friction (µ) by taking an average of the data between 40 and 50 mm along the track length (where the values for µ had typically reached a plateau and where there is no longer believed to be any contribution from static friction behaviour which might occur at < *ca.* 10 mm) and using Eq. 1. All LFT tests were carried out in triplicate with mean values quoted (errors quoted are standard deviations from the mean).

$$\mu = \text{Pulling Force} / (2 \times \text{Normal Force}) \quad \text{Eq. 1}$$

Wear was assessed using digital photographs of the wear tools and by confocal microscopy using a Nanofocus µSurf Mobile on 2.1mm x 2.1mm areas of steel samples at 20x magnification. The data were plotted using Mountains software, version 7.3.

3. Results and Discussion

3.1 Lubricity Compounds and Substrate

Lubricity compounds typically contain three main functionalities; a linker group to fix the compound to the substrate surface, a long (usually alkyl) chain which reduces surface energy and side groups attached to the long chain (Scheme 1a). In this work, three compounds have been studied all of which possess a carboxylic acid linker group. However, the compounds chosen vary in the length of alky chain and side groups they possess. Thus, perfluorooctanoic acid possesses only C-F side groups and consists of an 8 carbon chain and is subsequently labelled here as **C8**. By comparison, lauric and stearic acid possess only C-H side groups but consist of twelve and eighteen carbon chains and so are labelled here as **C12** and **C18**, respectively. The substrate chosen for lubricity testing (DX56) is galvanized steel with low surface roughness, which is designed for use in the automotive sector. The DX56 surface consists of a galvanic coating weight of 50-90 g m^{-2} which corresponds to a thickness of *ca.* 9-13 µm made up of 99.7 wt% Zn and 0.3 wt% Al. Thus, the outer surface of the DX56 substrate is expected to consist of a thin layer of predominantly ZnO.

Scheme 1 here

3.2 Infrared Spectroscopy

After removing surface oil from the DX56 substrate, the lubricity compounds have been deposited onto the steel by dip coating. IR data for **C8**-coated steel show a broad peak at *ca.* 3250cm^{-1} (Fig. 1**)** which also appears in the spectrum of the neat acid (ESI Fig. 2). This is ascribed to inter-molecular H-bonding between the carboxylic acid moieties, suggesting there is physisorbed acid on the surface. However, the υC=O of neat **C8** is not observed at 1711cm^{-1} in the coated sample. Instead, two bands are observed at 1727 and 1652cm^{-1} (Fig. 1), which are assigned as υC=O and the asymmetric υCO_2 of the carboxylate linker of **C8** bound to the oxide surface in the bridging coordination mode[21]. Bands at 1430 and 1366cm^{-1} are assigned to the symmetric υCO_2 of the bridging coordination mode and tentatively to the asymmetric υCO_2 of carboxylates bound through monodentate coordination[21]. Whilst this suggests multiple coordination modes for **C8**, no bands for the monodentate carboxylate symmetric stretching vibration are observed.

Fig. 1 here

Previous studies have shown that carboxylic acids can chemisorb to metal oxide surfaces through covalent ester bonds[7, 10, 21] and that physisorbed molecules can be

readily removed by solvent rinsing[7, 8, 22]. To study this, acetone rinsing shows that, whilst no carbonyl or carboxylate stretching bands are observed, υC-F are present between 1358 and 1140cm^{-1} (ESI Fig. 3). This confirms that **C8** remains adsorbed and suggests that the dipole moments of the carboxylate-related bands may be oscillating parallel to the surface and so are invisible in the IR spectrum[23]. Further evidence for this is that, after $NaOH_{(aq)}$ treatment to de-esterify the **C8**, there are no carboxylate or C-F bands in the spectrum confirming that all the remaining **C8** has been desorbed (ESI Fig. 4).

IR spectra for **C12**- and **C18**-coated DX56 show υC-H at 3000-2800cm^{-1} (Fig. 1). Both spectra show intense υC=O bands at *ca.* 1700cm^{-1} and weaker carboxylate asymmetric υCO_2 at *ca.* 1550cm^{-1} whilst symmetric υCO_2 bands are expected to be coincident with carboxylate-related bands from physisorbed **C12** or **C18**. The signals observed are ascribed to non-dissociated **C12** and **C18** acids along with surface-bound esters[7, 10, 13] suggesting that both of these coatings contain physi- and chemisorbed **C12** and **C18**, respectively. For both acetone rinsed coatings, symmetric and asymmetric υCO_2 bands are observed at 1542 and 1400cm^{-1}, respectively along with a band ascribed to methylene scissoring at 1465cm^{-1} [24] (ESI Fig. 3). These bands confirm that esterified, chemisorbed **C12** and **C18** remain on the surface whilst any physisorbed material is removed. Analysis of Δυ between $\upsilon\ CO_{2\ asym}$ and $\upsilon\ CO_{2\ sym}$ gives a value of *ca.* 140 cm^{-1} for **C12** and **C18** coatings which is consistent with carboxylate groups coordinating to surface atoms in a bridging coordination mode[25]. Such sorption has been observed in prior studies whereby bonding proceeds through coordination of both carboxylate oxygen atoms to two different surface sites [4, 10, 22]. Scheme 1b shows bidentate coordination of **C8**, **C12** and **C18** on a substrate surface.

3.3 Scanning Electron Microscopy (SEM)

SEM for "as received" DX56 steel shows contamination ascribed to oil deposited before transit to minimize corrosion. After cleaning, SEM confirms oil removal (ESI Fig. 5a). After dip coating DX56 in $Ti(OiPr)_4$ solution, the surface topography reduces due to the deposition of a TiO_2 film whilst EDX data confirms Ti is present (ESI Fig. 5b). For the lubricity compounds, the **C8** surface shows few new features beyond the TiO_2-coated DX56 although the surface appears darker suggesting that the coating interacts differently with the electron beam (Fig. 2a). The **C12** surface shows more surface features suggesting a thicker film has been deposited (Fig. 2b) whilst the **C18** surface shows needle-like structures (Fig. 2c) suggesting stearic acid has deposited as a separate phase.

AFM data (ESI Fig. 7) of 10 x 10 μm areas of the samples show low surface topography for the DX56 substrate (± 10 nm). After $Ti(OPr)_4$ treatment, new features are observed which are 200-250 nm in height and which are ascribed to TiO_2 particles that we observe in the SEM. After deposition of **C8** (ESI Fig. 8), a much higher surface topography is observed (± 1,000 nm) but this drops to ± 80 nm after rinsing in line with removal of some physisorbed **C8**. However, the surface topography is still much greater than the substrate suggesting that a model similar to Fig. 6d is occurring for **C8**. For the **C12** surface, the surface topography is ± 200 nm but this drops to ± 10 nm barring

spikes for residual TiO_2 particles (ESI Fig. 9). However, the WCA remains hydrophobic and the coefficient of friction remains low. This suggests monolayer **C12** coverage represented in Fig. 6c. The as-deposited **C18** surface shows angular particles with surface topography ± 80 nm (ESI Fig. 10). XRD shows that these particles are crystalline indicating phase separation of excess stearate material (ESI Fig. 11). After acetone rinsing, these particles disappear but the surface topography (± 50 nm) suggests multiple layers of **C18** remain.

Fig. 2 here

3.4 X-ray photoelectron spectroscopy (XPS)

XPS data for cleaned DX56 show Zn $2p_{1/2}$ and Zn $2p_{3/2}$ photoelectron peaks at 1021.2 and 1044.0eV, respectively[26-28] as well as a weak Al 2p photoelectron peak at 73.9eV (ESI Fig. 12 and 13). This is expected as Al is added to the galvanic Zn coating to control the structure of the intermetallic formed at the interface between the Zn coating and the underlying steel[26]. A broad O 1s signal at 531.70eV also confirms the presence of surface oxide[26]; mostly ZnO for the DX56 substrate. Fig. 3 shows that, after $Ti(OiPr)_4$ treatment, Ti $2p_{1/2}$ and Ti $2p_{3/2}$ peaks are observed at 458.0 and 463.7eV in agreement with previous studies[29-31]. The O 1s signal also splits into two peaks at 531.2 and 529.5eV for ZnO and the newly formed TiO_2[32].

TiO_2-coated DX56 treated with **C8** shows an intense F 1s photoelectron peak at 689.9eV (ESI Fig. 14) confirming the presence of fluorine on the surface[33]. A C 1s peak centred at *ca.* 291.8eV de-convolutes to reveal the presence of C=O, CF_2, and CF_3 moieties for the fluorinated carboxylic acid[34] (Fig. 3). For the TiO_2-coated DX56 treated with **C12** or **C18**, the C 1s peak envelopes de-convolutes to reveal the presence C=O, C-CO_2 and C-C components (Fig. 3) as expected for these alkyl carboxylates. The assignments are in line with related studies for carboxylic acids binding to steel[13] or iron oxide surfaces[10].

As a way to compare the loadings of **C8**, **C12** and **C18**, the at% of C 1s was found to be 31.6%, 66.4% and 91.7%, respectively. In this context, for typical photo-electron kinetic energies (10-1000eV), mean free path escape depths are 1-10nm corresponding to 2-10 monolayers[35]. Thus the lower at% of carbon and the higher intensity Zn 2p peaks for **C8** (3.7 at% Zn) suggest either poor coverage with substantial surface area not occupied by **C8** and/or a **C8** loading of 1-2 monolayers. For **C12**, the at% of C more than doubles whilst the Zn drops accordingly (1.2 at% Zn) suggesting either a higher coverage of **C12** and/or a multilayer **C12** loading. By comparison, the **C18** coating shows the highest at% for C along with the lowest intensity Zn 2p peaks (0.2 at% Zn) which suggests almost complete coverage of **C18** on the surface and/or a many multilayer loading of **C18**. To further understand loadings on TiO_2 surfaces, **C8**, **C12** or **C18** were sorbed onto Degussa P25 powder and then thermal gravimetric analysis (TGA) was measured to study the mass loss following their combustion (ESI Fig. 15 and ESI Table 1). From these data, the mass of **C8**, **C12** or **C18** initially sorbed onto P25 was found to be 10.9%, 71.0% and 78.8%, respectively. After acetone washing, the sorbed masses of C8, C12 or C18 drop to 8.7%, 24.9% and 44.5%,

respectively. Whilst these data show very little change in the **C8** loading after washing, the **C12** loading drops by almost two-thirds and **C18** drops by almost a half. These data correlate strongly with the IR data which lower peak intensities for the lubricity compounds (**C8**, **C12** or **C18**) spectra after acetone washing.

Assuming 10mg of coated P25 TiO_2, the acetone-washed loadings correspond to 2.1μmoles, 12.4μmoles and 15.6μmoles of **C8**, **C12** or **C18**. Given that P25 has a surface area of *ca.* $50m^2g^{-1}$ [15], a 10mg sample has an surface area of $0.5m^2$. The cross-sectional area of **C18** have been reported to be $20.7Å^2$ [36]. Thus, to form a monolayer of **C18** on 10mg of P25 should require 4.0μmole of **C18**. Given that C8 and C12 both possess a similar carboxylate linkers to **C18**, it can be assumed that their cross-sectional areas should also be similar and thus should require similar loadings to achieve monolayer coverage. Thus, these data suggest an average of *ca.* 0.5, 3.0 and 4.0 monolayer coverage for **C8**, **C12** and **C18**, respectively.

Fig. 3 here

3.5 Water contact angle measurements

The water contact angle (WCA) of "as received" DX56 galvanized steel were highly variable, which is ascribed to surface oil used to reduce corrosion in transit. After thorough cleaning, DX56 displays a more consistent WCA (55 ± 5^o) (Fig. 4). Whilst the WCA did not vary after $Ti(OiPr)_4$ treatment, the addition of either **C12** or **C18** generates hydrophobic surfaces with WCA of 88 ± 3^o and 110 ± 8^o respectively suggesting these surfaces have been covered by the carboxylic acids. Similar WCA values have been reported for alkythiols on gold[37], alkylsilanes on paper[38] and carboxylic acids on mica[39]. By comparison, the equivalent **C8** samples display hydrophilic WCA similar to the TiO_2-coated and uncoated DX56 (58 ± 7^o). This may be due to lower or less homogeneous **C8** surface coverage or potentially the formation of a **C8** bi-layer whereby a second layer of **C8** molecules orient their carboxylic acid groups away from the surface, increasing interaction with droplet water molecules (Fig. 6d). However, the TGA data for **C8** adsorbed onto P25 TiO_2 show only 0.5 monolayer loading which suggests low coverage is the main reason for the low WCA value. To test this further, the WCA of acetone rinsed samples were also measured to ensure the removal of any physisorbed **C8**, **C12** or **C18**.

As expected, acetone rinsing did not affect the WCA of DX56 or TiO_2-coated DX56. However, acetone rinsing **C8**-coated samples does increase WCA to 75 ± 6^o, suggesting more of the surface consists of C-F terminated chains. Similarly, the WCA of **C12** increases to 108 ± 6^o in line with a more hydrophobic surface. In this case, removing physisorbed **C12** increases the proportion of the surface which is C-H alkyl terminated. Finally, rinsing **C18**-coated samples does not change the WCA which suggests that, prior to rinsing, the surface was already alkyl terminated (Fig. 6d).

Fig. 4 here

3.6 Linear Friction Testing (LFT)

Coefficients of friction (μ) have been determined using LFT which is an aggressive tribological test, during which the galvanized coating is completely removed (Fig. 5a). Fig. 5b shows how μ varies along the samples. Cleaned DX56 shows the highest friction during the first 10mm (μ > 0.35), which then drops to between μ = 0.22-0.30. The initial increased friction observed may be due to several reasons including stick-slip behaviour resulting from substantial differences in roughness across the substrate surface, running in behaviour being influenced by surface roughness, the presence of a built-up transfer layer or adhesive friction between the tool and substrate. The dynamic value of μ (0.23) for TiO_2-coated DX56 suggests that adding TiO_2 to the surface does not influence lubricity. For the coated samples, μ displays little variation along the samples and this absence of variable friction behaviour suggests that surface coverage is sufficiently homogeneous to overcome substrate surface roughness.

Interestingly, the **C8** coating displays a dynamic μ of 0.20, which remains the same after acetone rinsing (Fig. 5c). The high friction observed is in agreement with previous studies; high μ values have also been observed for perfluorinated carboxylic acids on silicon[40] and for perfluorinated phosphonates on copper[11]. High μ values have also been observed on related systems involving fluorinated[41] or perfluorinated[11, 40] monolayers; discussions in the literature have attributed this to a number of factors including lower packing densities, relative to their hydrocarbon analogues, the molecular size of terminal groups, and molecular disorder in the molecular films[42]. By comparison, the **C12** and **C18** coatings give μ values of 0.11 and 0.10 (Fig. 5c). This is in agreement with previously reported studies where large reductions in μ values have been reported for phosphonates on copper[11], silanes on silicon[10], and carboxylic acids on Al[7] and steel[9], wherein it is believed that energy dissipation occurs through steric quenching between neighbouring alkyl chains[43]. After acetone rinsing, the dynamic μ of **C12** and **C18** coatings remain the same suggesting that sufficient chemisorbed material remains to imbue lubricity to these surfaces. Prior studies have shown that the stabilization energy incurred through increasing the number (n) of methylene (CH_2) groups in a chain saturates between n = 8-10[43].

Analysis of the wear tools using digital photography (ESI Fig. 16) shows that, after LFT testing, there is less build-up of larger zinc flakes on the wear tools that had been used to test the **C12** and **C18** coatings compared to the uncoated FF substrate which is in agreement with the LFT data that these coatings reduce the coefficient of friction for these samples. Also in line with the wear tool imaging and LFT data, confocal microscopy (ESI Fig. 17) shows smaller scratches for the **C12** and **C18** coatings which suggests that less material has been removed and hence that the wear is lower for these coatings.

A plot of μ *vs* WCA (Fig. 6a) shows that a negative correlation exists between the coefficient of friction and surface wettability. This suggests that it should be possible to predict substrate lubricity from contact angle data because, whilst WCA data only provide averaged information across the surface area of the water droplet used, these data do provide a measure of the extent of functionalization of surfaces. This is key because it has been reported that close-packed monolayers can facilitate low friction behaviour on some surfaces by enabling energy dissipation by steric quenching

between neighbouring alkyl chains during tribological contact[43]. Thus, whilst the correlation between WCA and μ effectively reflects surface coverage, the observed trend cannot take into account multiple layers and/or the molecular orientation within the surface films. However, with these provisos, our data do show that WCA can be used as a rapid screening method to identify substrate friction properties.

Applying this to our samples, for **C8** this explains the high value of μ because the low surface coverage of **C8** reduces inter-molecular steric quenching whilst uncoated areas possess no effective barrier during sliding (Fig. 6c). By comparison, SEM and XPS data for the unrinsed **C12** and **C18** samples, show that the films are thicker than **C8**, show higher surface coverage and contain both physisorbed carboxylic acids and chemisorbed carboxylates (Fig. 6c,d). Therefore, it is plausible to suggest that, prior to rinsing, the films act as more like barrier coatings, preventing interfacial contact between the substrate and tool during tribological contact. Interestingly, μ does not vary for these samples after solvent rinsing even through IR data shows that only chemisorbed carboxylates remain on the surface. This can be ascribed to the chemisorbed **C12** and **C18** carboxylates forming more ordered films where the alkyl chains are sufficiently ordered and close packed to enable steric quenching between neighbouring chains and thus to reduce frictional forces. This model for the structures of the coatings is shown (Fig. 6b-d). This shows that the TiO_2 layer formed as a result of dip coating process produces a partially covered surface. Between the TiO_2-rich areas is ZnO from oxidation of the Zn-rich galvanic layer. Where metal oxide is present, the carboxylic acids can then chemisorb through esterification to surface hydroxide groups to form a monolayer where the alkyl groups orient themselves away from the substrate surface. However, if the loading is high enough, additional layers can physisorb as shown in Fig. 6d. Where free carboxylic acid groups orient themselves away from the substrate surface, it is possible for this to lower the WCA and increase μ. Whilst solvent rinsing can remove this physisorbed material, only de-esterification using strong base can remove the chemisorbed species.

Fig. 5 here

4. Conclusions

Controlling surface lubricity is key for reducing wear during metal forming. At the same time, reducing waste and improving surface finish are driving the need to avoid oil-based lubrication and to reduce the substrate surface roughness required for such emulsions to work. Our approach to these problems has been to develop films which imbue inherent lubricity to metal surfaces. Whilst previous reports have suggested this is possible by pre-etching the substrate to remove surface oxide, we have instead attached monolayers of oriented alkyl chains directly to the oxide surface through carboxylate linkers. This approach is both cost effective and scaleable and we have used it on substrates up to 30cm in dimension. We have also screened different alkyl chain lengths and side groups (C-F *vs* C-H) and found that the initial deposits are thicker, multi-layer films but that acetone washing removes physisorbed material for all the compounds tested. However, **C12** (lauric acid) is the most effective in terms of

monolayer coverage, WCA and coefficient of friction. By comparison, **C8** (octanoic acid) shows low WCA and high μ whilst, for **C18** (stearic acid), phase-separated particles of **C18** are observed but, even after acetone rinsing, there is still too much material resulting in multi-layer surface films. Whilst stearic acid is not expensive this is still inefficient and wastes material. Through analysis of these data, it was also found that water contact angles can act as an effective screening method for compounds that could increase the surface lubricity.

Fig. 6 here

References

1. Allen SJ, Mahdavian SM, The effect of lubrication on die expansion during the deep drawing of axisymmetrical steel cups, *J. Mater. Process. Tech*., 2008; **199**: 102-107. DOI:10.1016/j.jmatprotec.2007.08.005.
2. Abe Y, Ohmi T, Mori K, Masuda T, Improvement of formability in deep drawing of ultra-high strength steel sheets by coating of die, *J. Mater. Process. Tech*., 2014; **214**: 1838-1843. DOI:10.1016/j.jmatprotec.2014.03.023.
3. Stepina V, Vesely V, in *Lubricants and Special Fluids*, Elsevier, Amsterdam, 1992, 2.
4. Lascoe OD, in *Handbook of Fabrication Processes*, 5th Ed., 1988, ASM Int., 264.
5. Oberg E, Jones FD, Horton HL, Ryffel HH, in *Machinery's Handbook*, 29th Ed., 2012, Ind. Press, NY, 1372.
6. Davies G, in *Materials for Automobile Bodies*, Elsevier, Oxf., 2012, 113.
7. Zhang Q, Wan Y, Li Y, Yang S, Yao W, Friction reducing behavior of steric acid on a textured aluminium substrate, *Appl. Surf. Sci.*, 2013; **280**: 545-549. DOI: 10.1016/j.apsusc.2013.05.024
8. Ruths M, Lundgren S, Danerlöv K, Persson K, Friction of fatty acids in nanometer-sized contacts of different adhesive strength, *Langmuir,* 2008; **24**; 1509-1516. DOI: 10.1021/la7023633.
9. Loehlé S, Matta C, Minfray C, Le Mogne T, Iovine R, Obara Y, Miyamoto A, Martin JM, Mixed lubrication of steel by C18 fatty acids revisited. Part I: toward the formation of carboxylate, *Tribol. Int*., 2015; **82**; 218-227. DOI: 10.1016/j.triboint.2015.08.036.
10. De Palma V, Tillman N, Friction and wear of self-assembled trichlorosilane monolayer films on silicon, *Langmuir*, 1989; **5**: 868-872. DOI: 10.1021/la00087a049
11. Hoque E, DeRose JA, Bhushan B, Hipps KW, Low adhesion, non-wetting phosphonate self-assembled monolayer films formed on copper oxide surfaces, *Ultramicroscopy*, 2009; **109**: 1015-1022. DOI: 10.1016/j.ultramic.2009.03.033
12. Liu H, Bhushan B, Investigation of nanotribological properties of self-assembled monolayers with alkyl and biphenyl spacers, *Ultramicroscopy*, 2002, **91**: 185-202. DOI: 10.1016/S0304-3991(02)00099-2.

13. Sahoo RR, Biswas SK, Frictional response of fatty acids on steel, *J. Colloid Interface Sci*., 2009; **333**:707-718. DOI: 10.1016/j.jcis.2009.01.046.
14. Holliman PJ, Vaca Velasco B, Butler I, Wijdekop M, Worsley D, Studies of dye sensitisation kinetics and sorption isotherms of Direct Red 23 on titania. *Int. J. Photoenergy*, 2008; 1-8. DOI: 10.1155/2008/ 827605.
15. Charbonneau C, Holliman PJ, Davies M, Watson T, Worsley D, Facile self-assembly and stabilization of metal oxide nanoparticles, *J. Colloid Interface Sci*., 2015; **442**: 110-119. DOI: 10.1016/j.jcis.2014.11.042.
16. Holliman PJ, Al-Salihi KJ, Connell A, Davies ML, Jones EW, Worsley DA, Development of selective, ultra-fast multiple co-sensitization to control dye loading in dye-sensitized solar cells, *RSC Adv*., 2014; **4**; 2515-2522. DOI: 10.1039/c3ra42131g
17. Connell A, Holliman PJ, Jones EW, Furnell L, Kershaw C, Davies ML, Gwenin CD, Pitak MB, Coles SJ, Cooke G, Multiple linker half-squarylium dyes for dye-sensitized solar cells; are two linkers better than one? *J. Mater. Chem. A*, 2015; **3**; 2883-2894. DOI: 10.1039/C4TA06896C
18. Beake BD, Leggett GJ, Variation on frictional forces in air with the composition of heterogeneous organic surfaces, *Langmuir*, 2000; **16**: 735-739. DOI: 10.1021/la990782d
19. Lundgren SM, Ruths M, Danerlöv K, Persson K, Effects of unsaturation on film structure and friction of fatty acids in a model base oil, *J. Colloid Interface Sci*., 2008; **326**: 530-536. DOI: 10.1016/j.jcis.2008.05.068
20. Trzepiecinski T, Bazan A, Lemu HG, Frictional characteristics of steel sheets used in automotive industry, *Int. J. Automotive Tech*., 2015; **16**: 849-863. DOI: 10.1007/s12239-015-0087-1
21. Przedlacki M, Kajdas C, Tribochemistry of fluorinated fluids hydroxyl groups on steel and aluminium surfaces, *Tribol. Trans*., 2006; **49**: 202-214. DOI: 10.1080/05698190500544676
22. Taheri P, Wielant J, Hauffman T, Flores JR, Hannour F, de Wit JHW, Mol JMC, Terryn H, A comparison of the interfacial bonding properties of carboxylic acid functional groups on zinc and iron substrates, *Electrochim. Acta*, 2011; **56**: 1904-1911. DOI: 10.1016/j.electacta.2010.10.079
23. Greenler RG, Snider DR, Witt D, Sorbello RS, The metal-surface selection rule for infrared spectra of molecules adsorbed on small metal particles, *Surf. Sci*., 1982, **118**: 415-428. DOI: 10.1016/0039-6028(82)90197-2
24. Ozturk S, Balkose D, Okur S, Umemura J, Effect of humidity on electrical conductivity of zinc stearate nanofilms, *Colloids Surf. A: Physicochem. Eng. Aspects*, 2007; **302**: 67-74. DOI: 10.1016/j.colsurfa.2007.01.039.
25. Kutscher JS, Gericke A, Hűhnerfuss H, Effect of bivalent Ba, Cu, Ni and Zn cations on the structure of octadecanoic acid monolayers at the air-water interface as determined by external infrared reflection-absorption spectroscopy, *Langmuir*, 1996; **12**: 1027-1034. DOI: 10.1021/la950731q.

26. Feliu Jr. S, Barranco V, XPS study of the surface chemistry of conventional hot-dip galvanized pure Zn, galvanneal and the Zn-Al alloy coatings on steel, *Acta Materialia*, 2003; **51**: 5413-5424. DOI: 10.1016/S1359-6454(03)00408-7
27. Lebrini M, Fontaine G, Gengembre L, Traisnel M, Lerasle O, Genet N, Corrosion behaviour of galvanized steel and electroplating steel in aqueous solution: AC impedance study and XPS, *Appl. Surf. Sci*., 2008; **254**: 6943-6947. DOI: 10.1016/j.apsusc.2008.04.112
28. Arenas MA, García I, Damborenea J, X-ray photoelectron spectroscopy study of the corrosion behaviour of galvanised steel implanted with rare earths, *Corrosion Sci.,* 2004; **46**:1033-1049. DOI: 10.1016/S0010-938X(03)00193-8
29. Pazokifard S, Farrokhpay S, Mirabedini M, Esfandeh M, Surface treatment of TiO_2 nanoparticles via sol-gel method: effect of silane type on the hydrophobicity of the nanoparticles, *Progr. Org. Coatings*, 2015; **87**: 36-44. DOI: 10.1016/j.porgcoat.2015.04.021
30. Al-Kandari H, Mohamed AM, Al-Kharafi F, Katrib A, XPS-UPS, ISS characterization studies and the effect of Pt and K addition on the catalytic properties of $MoO_{2-x}(OH)_y$ deposited on TiO_2, *J. Electron Spec. Related Phenom.*, 2011; **184**: 472-478. DOI: 10.1016/j.elspec.2011.07.001.
31. Kruse N, Chenakin S, XPS characterization of Au/TiO_2 catalysts: binding energy assessment and irradiation effects, *Appl. Catal. A: Gen.*, 2011; **391**: 367-376. DOI: 10.1016/j.apcata.2010.05.039.
32. Hanawa T, Ota M, Calcium phosphate naturally formed on titanium in electrolyte solution, *Biomater*., 1991; **12**: 767-774. DOI: 10.1016/0142-9612(91)90028-9
33. Beamson G, Briggs D, High Resolution XPS of Organic Polymers ESCA300 Database, 1992.
34. Suzuki S, Whittaker MR, Wentrup-Byrne E, Monterio MJ, L. Grondahl L, Adsorption of well-defined fluorine-containing polymers onto poly(tetrafluoroethylene), *Langmuir*, 2008; **24**: 13075-13083. DOI: 10.1021/la802300q
35. Seah MP, Dench WA, Quantitative electron spectroscopy of surfaces: a standard database for electron inelastic mean free paths in solids, *Surf. Interface Anal.*, 1979; **1**: 2-11. DOI: 10.1002/sia.740010103
36. Lane CL, Burton E, Crabb CC, Accurate molecular dimensions from stearic acid monolayers, *J. Chem. Ed*., 1984; **61**: 815. DOI: 10.1021/ed061p815
37. Nuzzo RG, Allara DL, Adsorption of bifunctional organic disulfides on gold surfacses, *J. Am. Chem. Soc.*, 1983; **105**: 4481-4483. DOI: 10.1021/ja00351a063
38. Oh MJ, Lee SY, Paik KH, Preparation of hydrophobic self-assembled monolayers on paper surfaces with silanes, *J. Ind. Eng. Chem.*, 2011; **17**: 149-153. DOI: 10.1016/j.jiec.2010.12.014.
39. Sauthiera G, Segurac JJ, Fraxedasa J, A. Verdaguer A, Hydrophobic coatings of mica by stearic acid vapor deposition, *Colloids Surf. A: Physicochem. Eng. Aspects*, 2014; **443**: 331-337. DOI: 10.1016/j.colsurfa.2013.11.031.

40. Singh RA, Yoon ES, Han HG, Kong H, Friction behaviour of chemical vapor deposited self-assembled monolayers on silicon wafer, *Wear*, 2007; **262**: 130-137. DOI: 10.1016/j.wear.2006.04.001.
41. Kim HI, Graupe M, Oloba O, Koini T, Imaduddin S, Lee TR, Perry SS, Molecularly specific studies of the frictional properties of monolayer films: a systematic comparison of CF_3-, $(CH_3)_2CH$-, and CH_3-terminated films, *Langmuir*, 1999; **15**: 3179-3185. DOI: 10.1021/la981497h.
42. Singh RA, Kim J, Yang SW, Oh JE, Yoon ES, Tribological properties of trichlorosilane-based one- and two-component self-assembled monolayers, *Wear*, 2008; **265**: 42-48. DOI: 10.1016/j.wear.2007.08.016.
43. Lio A, Charych DH, Salmeron M, Comparative atomic force microscopy study of the chain length dependence of frictional properties of alkanethiols on gold and alkylsilanes on mica, *J. Phys. Chem. B*, 1997; **101**: 3800-3805. DOI: 10.1021/jp963918e

List of Schemes and Figures

Scheme 1 Schematic of **C18** (top), **C12** (middle) or **C8** (bottom) bound to surface sites in bridging coordination mode. H atoms omitted for clarity.

Fig. 1 Infrared spectra of DX56 steel treated with (a) **C8** (b) **C12** or (c) **C18**.
● νC-H, ♣ νO-H, ▼ νC=O, † ν $CO_{2\ asym\ bridge}$, γ $\nu CO_{2\ sym\ bridge}$, ‡ $\nu CO_{2\ asym\ mon}$, α νC-F

Fig. 2 SEM data for TiO_2-coated DX56 steel treated with (a) **C8**, (b) **C12** or (c) **C18.**

Fig. 3 High resolution XPS spectra of TiO_2-coated DX56 substrate (a) Ti 2p and (b) O 1s are regions. Other spectra show C 1s regions after treatment with (c) **C8** or (d) **C12**. C=O (▼), C-CO_2 (♦), C-C (‡), CF_3 (■), CF_2 (●), COO (†), C-O (♣).

Fig. 4 (a) contact angles before (dark) and after (light) acetone rinsing and images for (b) TiO_2-coated DX56 and TiO_2-coated DX56 with (c) **C8**, (d) **C12** and (e) **C18**.

Fig. 5 (a) Image of sample after linear friction testing (LFT), (b) dynamic coefficient of friction (μ) data and (c) mean μ for substrates before (dark shading) or after (light shading) acetone rinsing. DX56 steel (grey), TiO_2-coated DX56 (black) and DX56 coated with **C12** (circles), **C18** (hashed) and **C8** (light grey).

Fig. 6 (a) Data for μ *versus* contact angle for DX56 steel (grey), TiO_2-coated DX56 steel (black), and DX56 steel with **C12** (dotted), **C18** (hashed) and **C8** (open). Circles are before acetone rinsing and triangles are after acetone rinsing, (b) schematic of lubricity compound, and proposed models for (c) monolayer and (d) multilayer coatings of carboxylic acids on DX56 steel.

Holliman Scheme 1

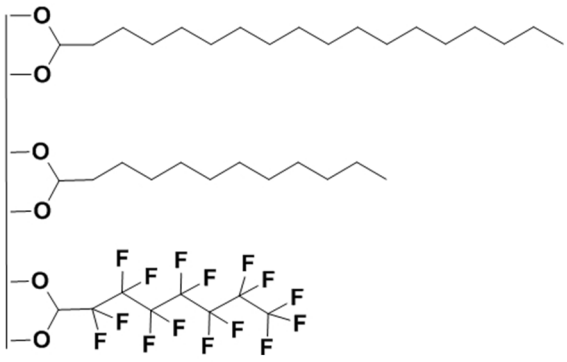

Scheme 1 Schematic of C18 (top), C12 (middle) or C8 (bottom) bound to surface sites in bridging coordination mode. H atoms omitted for clarity.
Scheme 1 here
190x275mm (96 x 96 DPI)

Holliman Fig. 1

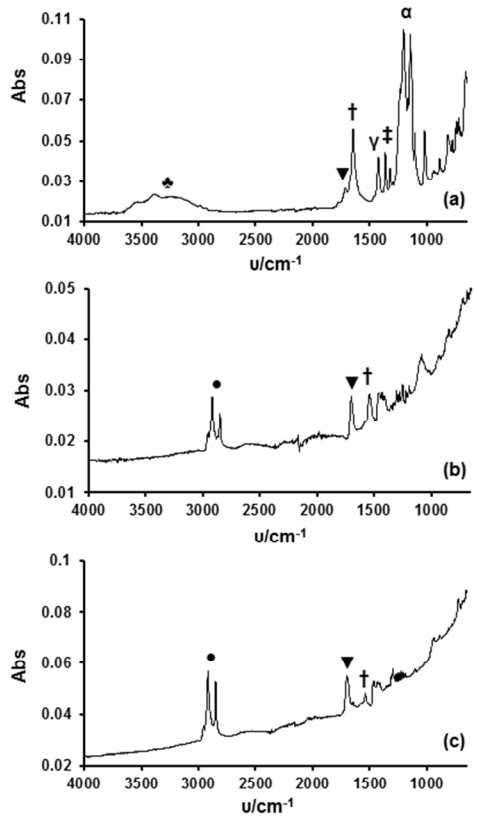

Fig. 1 Infrared spectra of DX56 steel treated with (a) C8 (b) C12 or (c) C18.
● vC-H, ♣ vO-H, ▼ vC=O, † ν CO_2 asym bridge, γ νCO_2 sym bridge, ‡ νCO_2 asym mon, α vC-F

Fig. 1 here
190x275mm (96 x 96 DPI)

Holliman Fig. 2

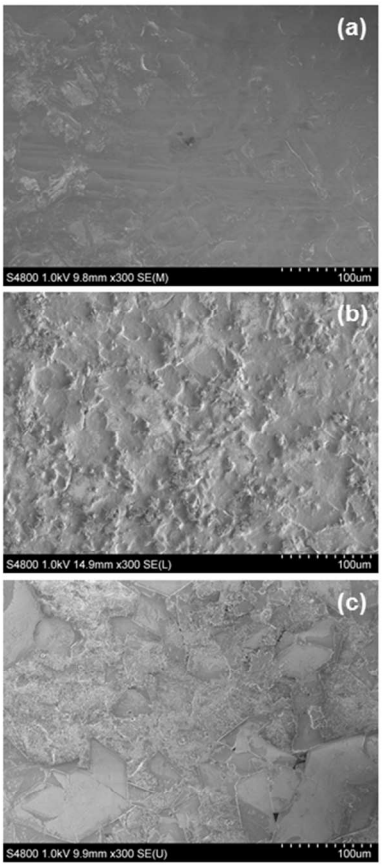

Fig. 2 SEM data for TiO2-coated DX56 steel treated with (a) C8, (b) C12 or (c) C18.
Fig. 2 here
190x275mm (96 x 96 DPI)

Holliman Fig. 3

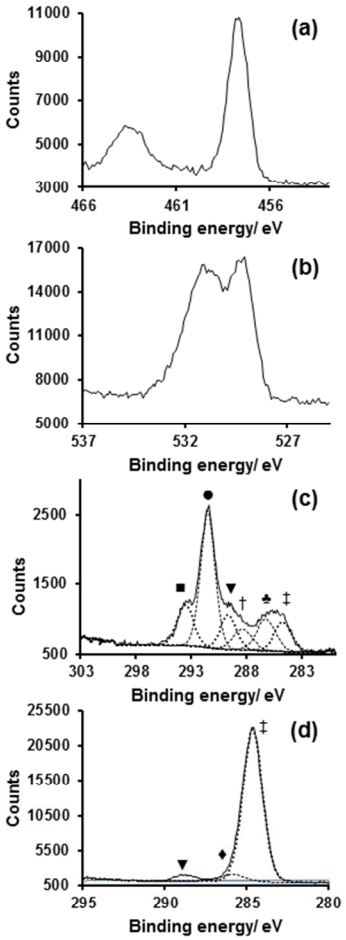

Fig. 3 High resolution XPS spectra of TiO_2-coated DX56 substrate (a) Ti 2p and (b) O 1s are regions. Other spectra show C 1s regions after treatment with (c) C8 or (d) C12. C=O (▼), C-CO_2 (♦), C-C (‡), CF_3 (■), CF_2 (●), COO (†), C-O (♣).

Fig. 3 here
190x275mm (96 x 96 DPI)

Holliman Fig. 4

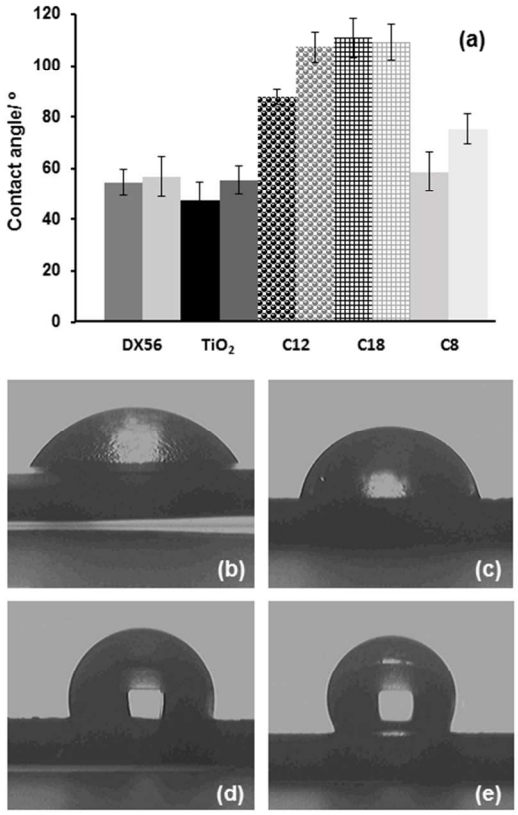

Fig. 4 (a) contact angles before (dark) and after (light) acetone rinsing and images for (b) TiO_2-coated DX56 and TiO_2-coated DX56 with (c) C8, (d) C12 and (e) C18.
Fig. 4 here
190x275mm (96 x 96 DPI)

Holliman Fig. 5

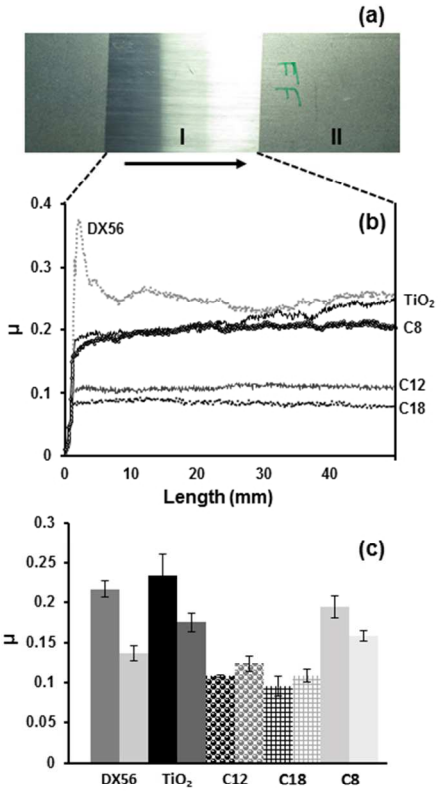

Fig. 5 (a) Image of sample after linear friction testing (LFT), (b) dynamic coefficient of friction (μ) data and (c) mean μ for substrates before (dark shading) or after (light shading) acetone rinsing. DX56 steel (grey), TiO_2-coated DX56 (black) and DX56 coated with C12 (circles), C18 (hashed) and C8 (light grey).
Fig. 5 here
190x275mm (96 x 96 DPI)

Holliman Fig. 6

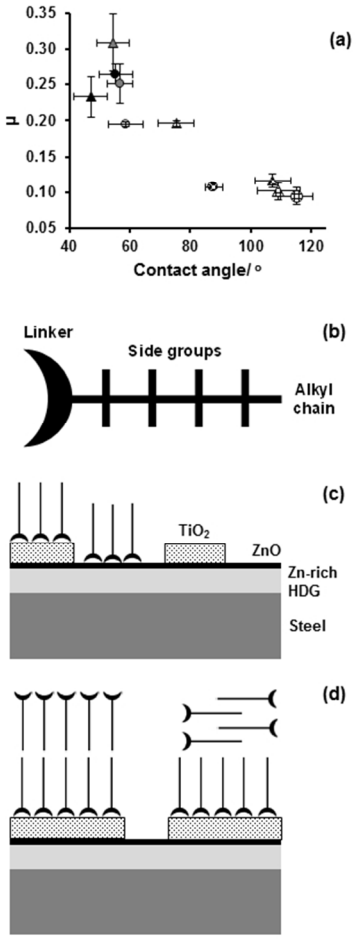

Fig. 6 (a) Data for μ versus contact angle for DX56 steel (grey), TiO_2-coated DX56 steel (black), and DX56 steel with C12 (dotted), C18 (hashed) and C8 (open). Circles are before acetone rinsing and triangles are after acetone rinsing, (b) schematic of lubricity compound, and proposed models for (c) monolayer and (d) multilayer coatings of carboxylic acids on DX56 steel.

Fig. 6 here
190x275mm (96 x 96 DPI)